

This is a pre-print version of the paper. Please cite the final version of the paper:

G. Di Martino, A. Iodice, D. Riccio, and G. Ruello, "Power Spectra of Very High Resolution SAR Amplitude Images of Urban Areas", *IEEE J. Sel. Topics Appl. Earth Observ.*, vol. 7, no. 7, pp. 2723-2731, July 2014. DOI: [10.1109/JSTARS.2014.2311174](https://doi.org/10.1109/JSTARS.2014.2311174).

IEEE Copyright notice. © 2014 IEEE. Personal use of this material is permitted. Permission from IEEE must be obtained for all other uses, in any current or future media, including reprinting/republishing this material for advertising or promotional purposes, creating new collective works, for resale or redistribution to servers or lists, or reuse of any copyrighted component of this work in other works.

Power Spectra of Very High Resolution SAR Amplitude Images of Urban Areas

Gerardo Di Martino, *Member, IEEE*, Antonio Iodice, *Senior Member, IEEE*,
Daniele Riccio, *Fellow, IEEE*, Giuseppe Ruello, *Member, IEEE*

Abstract — With the launch of COSMO/SkyMed and TerraSAR-X missions, very high resolution (VHR) Synthetic Aperture Radar (SAR) images of urban areas have become routinely available. In particular, in the spotlight acquisition mode, COSMO/SkyMed SARs are able to obtain a resolution even better than one meter. Accordingly, in principle a huge amount of information on objects present in the urban scenario can be extracted from such images; however, due to the involved interaction between incident electromagnetic wave and imaged scene, direct interpretation of VHR SAR images is not straightforward, and different methods to analyze them are being developed by the scientific community. In this paper, we explore the potentiality of using the power spectral density (PSD) of VHR SAR amplitude images of urban areas for information extraction. First, we propose a theoretical model of the PSD of such images, and then we test the validity of the developed model on COSMO/SkyMed spotlight SAR images of urban areas. Finally, some suggestions are provided on how the parameters of the obtained PSD can be exploited to extract useful information from VHR SAR amplitude images of urban areas.

Index Terms— Synthetic Aperture Radar (SAR), urban areas, power spectrum, very high resolution, parameter retrieval.

I. INTRODUCTION

STIMULATED by the availability of several Synthetic Aperture Radar (SAR) systems, with their well-known all-weather, illumination-independent functioning capabilities, the remote sensing scientific community is continuously increasing its efforts in the field of urban scenario monitoring via SAR images [1]-[22]. In recent years, the launch of COSMO/SkyMed and TerraSAR-X missions has made very high resolution (VHR) SAR images of urban areas routinely available: in particular, a resolution even better than one meter can be achieved by COSMO/SkyMed SAR images acquired in the spotlight mode.

In principle, from such images a huge amount of information can be extracted about objects present in the urban scenario. However, due to the significant presence of layover, shadowing, multiple reflections, and other involved electromagnetic

This work was supported by the Agenzia Spaziale Italiana (ASI) within the COSMO/SkyMed AO Project 2202 “Buildings Feature Extraction from Single SAR Images: Application to COSMO-SkyMed High Resolution SAR Images.”

The authors are with the Dipartimento di Ingegneria Elettrica e delle Tecnologie dell'Informazione, Università di Napoli Federico II, via Claudio 21, 80125, Napoli, Italy (e-mail: gerardo.dimartino@unina.it; iodice@unina.it; daniele.riccio@unina.it; ruello@unina.it).

scattering phenomena, direct interpretation of VHR SAR images of urban areas is not straightforward, and several techniques are being developed to analyze them: they are based on geometrical and electromagnetic modeling [1]-[6], image processing techniques [7]-[12], multi-temporal and/or multi-baseline image combination [13]-[20], and stochastic modeling [21]. All of these approaches analyze SAR images directly in the space domain; more recently, a spectral domain technique has been also proposed, based on Hough and Fourier transforms [22]. In this paper, we want to more systematically analyze the spectral domain approach. In particular, we want to explore the potentiality of using the power spectral density (PSD) of VHR SAR amplitude images of urban areas for information extraction.

Recently, a theoretical model of the PSD of SAR amplitude images of natural surfaces, described as fractional Brownian motion (fBm) fractal surfaces, was developed [23]-[24]. It was shown that the PSD of range cuts of such images holds a power-law behavior in a wide range of spatial frequencies, and that the exponent of this power law is related to the fractal dimension of the imaged surface [24]. It was also verified that, as expected, this PSD model does not apply to SAR images of urban areas [24]. However, a theoretical model for the PSD of SAR amplitude images of urban areas is not available. Actually, it is certainly not easy to predict the PSD of such SAR images, dominated by the involved combination of single scattering from terrain and buildings, and multiple scattering from dihedral and trihedral structures, especially if, as it happens for moderate- and low-resolution systems, they are simultaneously present in a single resolution cell. Nonetheless, for very high resolution SAR systems, such as COSMO/SkyMed in the spotlight acquisition mode, the resolution cell is so small that dihedral and trihedral returns dominate with respect to the single scattering background. Accordingly, a realistic description of VHR SAR amplitude images can be obtained by considering sparse brilliant points, or lines, over a dark background: the positions of these brilliant points and lines can be considered randomly distributed, unless they belong to a building façade, in which case an ordered, periodic spatial distribution is expected. Starting from this image model, in the following we construct a theoretical model of the PSD of range cuts of VHR SAR amplitude images, see Section II, and we test the validity of the obtained model on simulated data and on actual COSMO/SkyMed enhanced spotlight SAR amplitude images of the area of Naples, Italy, see Section III. In addition, we provide some suggestions on how the parameters of the obtained PSD can be exploited to extract useful information from VHR SAR amplitude images of urban areas, and we provide some relevant examples, see Section IV. Finally, some concluding remarks close the paper, see Section V.

II. THEORETICAL PSD MODEL

Let us consider a range cut of a portion of a VHR SAR amplitude image of an urban area. Many of the results that we will obtain also hold for azimuth cuts: when this is not the case, we will explicitly mention it.

In view of the considerations reported above, we can assume that the amplitude image is a superposition of sparse brilliant points and lines, so that an image range cut $i(r)$ can be expressed as a superposition of N pulses:

$$i(r) = \sum_{i=1}^N A_i p_i \left(\frac{r - r_i}{\delta_i} \right) , \quad (1)$$

where A_i , $p_i(\cdot)$, r_i and δ_i are the i -th pulse amplitude, shape, position and width, respectively. We are here assuming that $p_i(\cdot)$ is maximum and equal to unity when its argument is zero. The Fourier transform of (1) is

$$I(\eta) = \sum_{i=1}^N \exp(-j\eta r_i) A_i \delta_i P_i(\delta_i \eta) , \quad (2)$$

where η is the Fourier mate of r , and I and P_i are the Fourier transforms of i and p_i . Let us first consider the case of randomly distributed pulse positions, which is a reasonable assumption if no building façade is included in the considered portion of the SAR image. In this case, we can assume that r_i are mutually independent random variables, that they are statistically independent of random variables A_i and δ_i , and that their probability density function is uniform over the scene.

The PSD $S(\eta)$ of $i(r)$ is the statistical mean of the square modulus of $I(\eta)$:

$$S(\eta) = \left\langle \left| \sum_{i=1}^N \exp(-j\eta r_i) A_i \delta_i P_i(\delta_i \eta) \right|^2 \right\rangle = \sum_{i=1}^N \sum_{j=1}^N \left\langle \exp[-j\eta(r_i - r_j)] A_i A_j \delta_i \delta_j P_i(\delta_i \eta) P_j^*(\delta_j \eta) \right\rangle , \quad (3)$$

where $\langle \cdot \rangle$ stands for statistical mean and $*$ for complex conjugate.

In this case, even considering a single range cut realization (i.e., not performing any statistical mean), if we assume that there is no single dominant amplitude and that pulses' separations are greater than sensor resolution, we have that the complex terms in (3) tend to cancel out, except for those with $i=j$, that are all in phase. Accordingly, the overall sample PSD is approximated by the summation of the square modulus of the Fourier transform of single pulses. This approximate result becomes exact if we perform the statistical mean in (3). In fact, by exploiting the statistical description of r_i described above, we obtain

$$S(\eta) = \sum_{i=1}^N \sum_{j=1}^N \langle \exp[-j\eta(r_i - r_j)] \rangle \langle A_i A_j \delta_i \delta_j P_i(\delta_i \eta) P_j^*(\delta_j \eta) \rangle = \sum_{i=1}^N \langle A_i^2 \delta_i^2 |P_i(\delta_i \eta)|^2 \rangle . \quad (4)$$

Equation (4) states that the PSD is an averaged version of the square modulus of the pulse Fourier transform. If the different pulses have all the same shape and width, then the image cut PSD is directly proportional to the square modulus of the pulse Fourier transform.

If the considered portion of the image includes a building façade, then M out of the N pulses are regularly spaced, and they form a periodic pattern. In this case we can rewrite (1) as:

$$i(r) = \sum_{i=1}^{N-M} A_i p_i \left(\frac{r - r_i}{\delta_i} \right) + \sum_{m=0}^{M-1} A_0 p_0 \left(\frac{r - r_0 - m d}{\delta_0} \right) , \quad (5)$$

where the regular range spacing d of the façade structure can be related to the building inter-floor distance via the SAR incidence angle (for azimuth cuts, the regular azimuth spacing is also related to the building orientation with respect to the SAR line of flight, and, in addition, due to the cross-track look direction of SAR systems, the occurrence of regularly spaced pulses is less frequent). Accordingly, (2) becomes

$$I(\eta) = \sum_{i=1}^{N-M} \exp(-j\eta r_i) A_i \delta_i P_i(\delta_i \eta) + \exp(-j\eta r_0) A_0 \delta_0 P_0(\delta_0 \eta) \sum_{m=0}^{M-1} \exp(-j\eta d m) . \quad (6)$$

If, in addition to the above hypotheses on r_i , we also assume that r_0 is statistically independent of r_i , of A_0 , and of δ_0 , and that its probability density function is uniform over the scene, then we have

$$S(\eta) = \left\langle \left| \sum_{i=1}^{N-M} \exp(-j\eta r_i) A_i \delta_i P_i(\delta_i \eta) \right|^2 \right\rangle + \langle A_0^2 \delta_0^2 |P_0(\delta_0 \eta)|^2 \rangle \left| \sum_{m=0}^{M-1} \exp(-j\eta d m) \right|^2 . \quad (7)$$

The first term of (7) can be computed as in (3)-(4), whereas the summation in the second term can be expressed in terms of a Dirichlet kernel, thus obtaining:

$$S(\eta) = \sum_{i=1}^{N-M} \langle A_i^2 \delta_i^2 |P_i(\delta_i \eta)|^2 \rangle + \langle A_0^2 \delta_0^2 |P_0(\delta_0 \eta)|^2 \rangle > \left| \frac{\sin(\eta d M / 2)}{\sin(\eta d / 2)} \right|^2 . \quad (8)$$

Equation (8) states that the PSD is composed of two terms: the first one is an averaged version of the square modulus of the pulse Fourier transform, whereas the second one has peaks in correspondence of spatial frequencies

$$\eta_n = n \frac{2\pi}{d} . \quad (9)$$

These peaks are equal to $\langle A_0^2 \delta_0^2 |P_0(\delta_0 \eta_n)|^2 \rangle > M^2$ and have a width $\Delta\eta = \frac{2\pi}{dM}$.

Of course, (8) can be easily generalized to the case in which more than one façade are included in the considered portion of image. Note, however, that if in a large area many façades are present, with different orientations and inter-floor distances, the peaks may not emerge so that a spectrum of the kind of (4) is obtained.

A few last words are needed on the pulse shape. On a SAR amplitude image, if we assume ideal processing and if a single pulse is present that corresponds to a pointlike scatterer (for instance, a trihedral), then its shape is the absolute value of a sinc function:

$$p_i\left(\frac{r-r_i}{\delta_i}\right) = p_i\left(\frac{r-r_i}{a}\right) = \left| \frac{\sin\left(\pi \frac{r-r_i}{a}\right)}{\pi \frac{r-r_i}{a}} \right| , \quad (10)$$

where a is the SAR slant range resolution. If more than one pointlike scatterer is present, the corresponding (complex) pulses coherently sum up, so that in the amplitude image pulse shapes are modified with respect to (10), even in case their distances are greater than the resolution. However, the behavior of the pulse Fourier transform should remain similar to the Fourier transform of (10), which is discussed in the Appendix. More in general, for a non-ideal processing and/or if the pulse corresponds to a distributed scatterer with range size δ of the order of the range resolution (or, maybe, a group of very close pointlike scatterers covering a range size δ), then the pulse shape is not easily predictable and it may be possibly treated as a random process. However, some simulations, and some experimental evidence, see Section III, seem to indicate that a good approximation of the pulse shape is often given in this case by a Lorentzian function:

$$p_i\left(\frac{r-r_i}{\delta_i}\right) = \frac{1}{1+\left(\frac{r-r_i}{\delta_i}\right)^2}, \quad P_i(\delta_i\eta) = \pi \exp(-\delta_i|\eta|). \quad (11)$$

It is interesting to note that, in this latter case, according to (4) VHR SAR images of urban areas have an exponential spectrum, as opposed to SAR images of natural areas, which have a power-law spectrum. Accordingly, the plot of the former spectrum is a straight line in a linear-log plane, whereas the plot of the latter is a straight line in a log-log plane.

In Fig. 1 two examples of plots of PSD computed via (8) for Lorentzian pulses are reported.

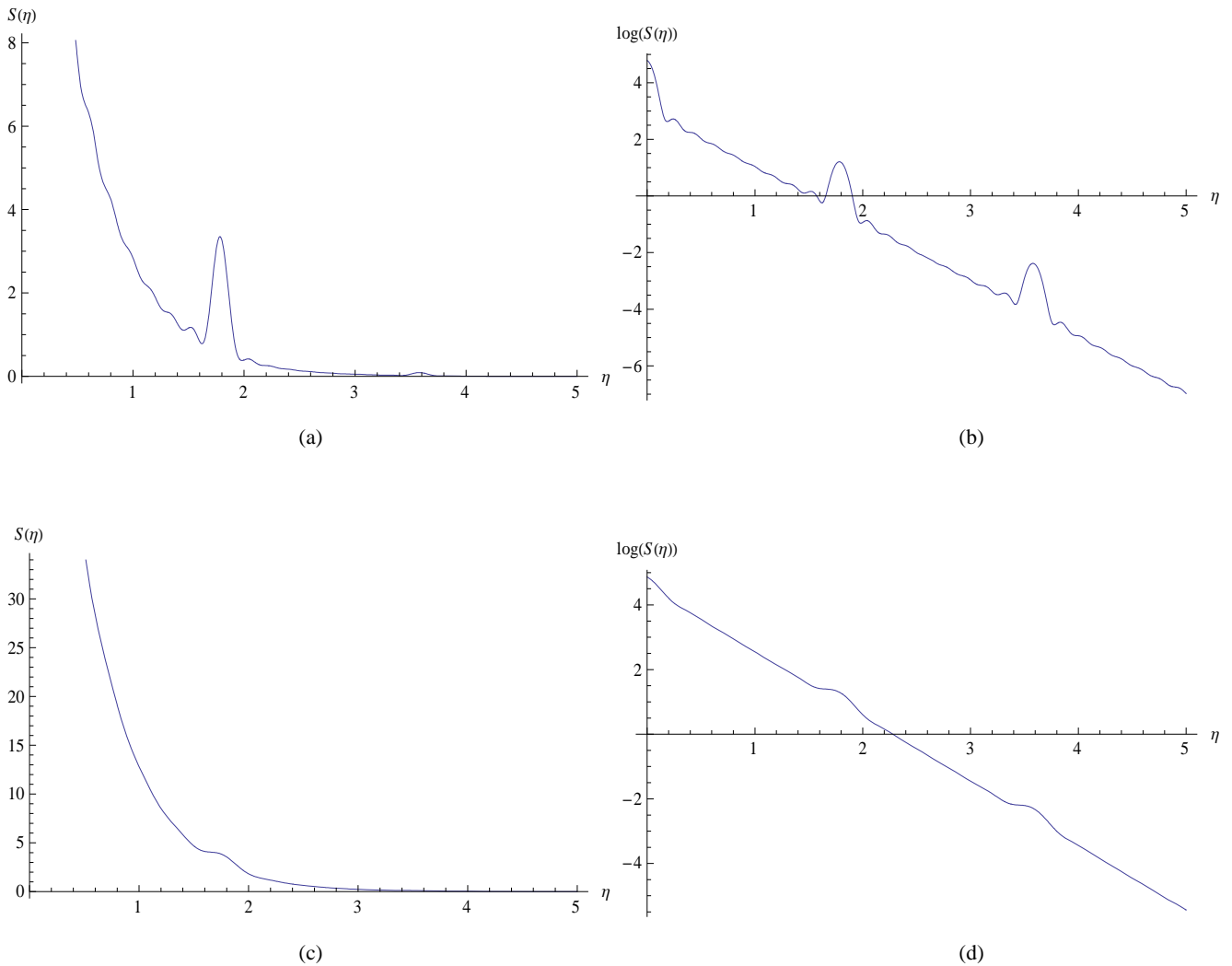


Fig. 1: Linear, (a), (c), and logarithmic, (b), (d), plots of the PSD of (8) normalized to $\langle A_i^2 \delta_i^2 |P_i(\delta_i\eta)|^2 \rangle = \langle A_0^2 \delta_0^2 |P_0(\delta_0\eta)|^2 \rangle$, for $\delta_i = 1$ m, $d = 3.5$ m, with $N=30$, $M=10$, (a)-(b), and $N=100$, $M=6$, (c)-(d). Abscissa η is measured in m^{-1} .

Finally, it is worth noting that, although the analysis above was referred to SAR amplitude images, with minor variations it also applies to SAR intensity images. All of the equations above still hold in this case, except for (10), in which the absolute value of the sinc function must be replaced by the square value of the sinc function.

III. EXPERIMENTAL RESULTS

In order to validate the PSD model developed in the previous section, we now estimate the PSD of some simulated and real SAR data. Since we expect to obtain PSDs that are rapidly decreasing, the employed spectral estimator must be robust with respect to spectral leakage [25]. Therefore, we use the Capon spectral estimator [25]-[26].

Let us first consider simulated data. In particular, we consider a set of 100 independent complex profiles, obtained as the (coherent) summation of 10 randomly spaced sinc pulses, with $a=0.679$ m, each multiplied by a complex factor with random amplitude and phase (in particular, a complex circular Gaussian distribution has been used). A random white noise is also added, with rms value equal to 1/100 of the pulses' rms amplitude. Sampling spacing is equal to 0.4 m. This simulates SAR complex profiles of images in which a few bright points corresponding to pointlike scatterers are presents. One sample profile is depicted in Fig. 2 (a). For each profile, the modulus is taken and its PSD is computed; then, the 100 computed PSDs are averaged. The logarithm of the obtained PSD is plotted in Fig. 2 (b). It is interesting to observe that, as we expected, this PSD is very similar to the Fourier transform of the absolute value of a sinc function, reported in the Appendix. The peak at spatial frequency $\eta/(2\pi) \cong 1.03 \text{ m}^{-1}$ is due to aliasing, as discussed in the Appendix.

In order to simulate the case in which pulses are due to groups of very close pointlike scatterers covering a range size comparable to resolution, we generate a new set of 100 independent complex profiles, obtained as the (coherent) summation of 10 randomly spaced pairs of sinc pulses, with $a=0.679$ m. The two sinc pulses of each pair are separated by a fraction of their width, namely of 0.34 m, and their amplitudes are one the double of the other. Each pair is multiplied by a complex factor with random amplitude and phase (again, a complex circular Gaussian distribution has been used). Random noise and sampling spacing are the same as in the previous example. The logarithm of the average PSD of the modulus of these profiles is plotted in Fig. 3. In this case, the plot is well approximated by a straight line in most of the spatial frequency range, which means that an approximately exponential PSD is obtained, as anticipated in the previous section. However, the presence of the peak at zero frequency and of the peak due to aliasing at about 1.03 m^{-1} show that the exponential approximation does not hold near the singular frequencies of the Fourier Transform of the absolute value of the sinc function, see Appendix.

Let us now move to real SAR data. We consider three COSMO/SkyMed enhanced spotlight SAR amplitude images of the area of Naples, Italy, acquired with look angles of 22, 31 and 44 degrees on September 4, August 17, and August 4 2011, respectively. The images present different values of resolution and pixel spacing: in particular, the resolution in azimuth-slant

range geometry is 1.08 m x 0.375 m for the 22° image, 1.09 m x 0.5 m for the 31° image, and 1.07 m x 0.679 m for the 44° image; the pixel spacing is 0.7 m x 0.31 m, 0.7 m x 0.32 m, and 0.7 m x 0.4 m, respectively. From each of these images we select three subsets, the first one relevant to a scene made up essentially of old or historical buildings located in the area of the Forcella neighborhood; the second one is relative to an area pertaining to the business district of Naples enclosing several very tall buildings; the last one is the layover area of one single skyscraper, i.e. the tallest of the three buildings forming the courthouse of Naples. In Fig. 4, as an example, we show a subset of the 44° image including the three areas of interest, which are marked in green, blue, and red, respectively. Note that on the other images the subsets cover approximately the same ground areas. For each subset we compute the PSDs of the range profiles and average them.

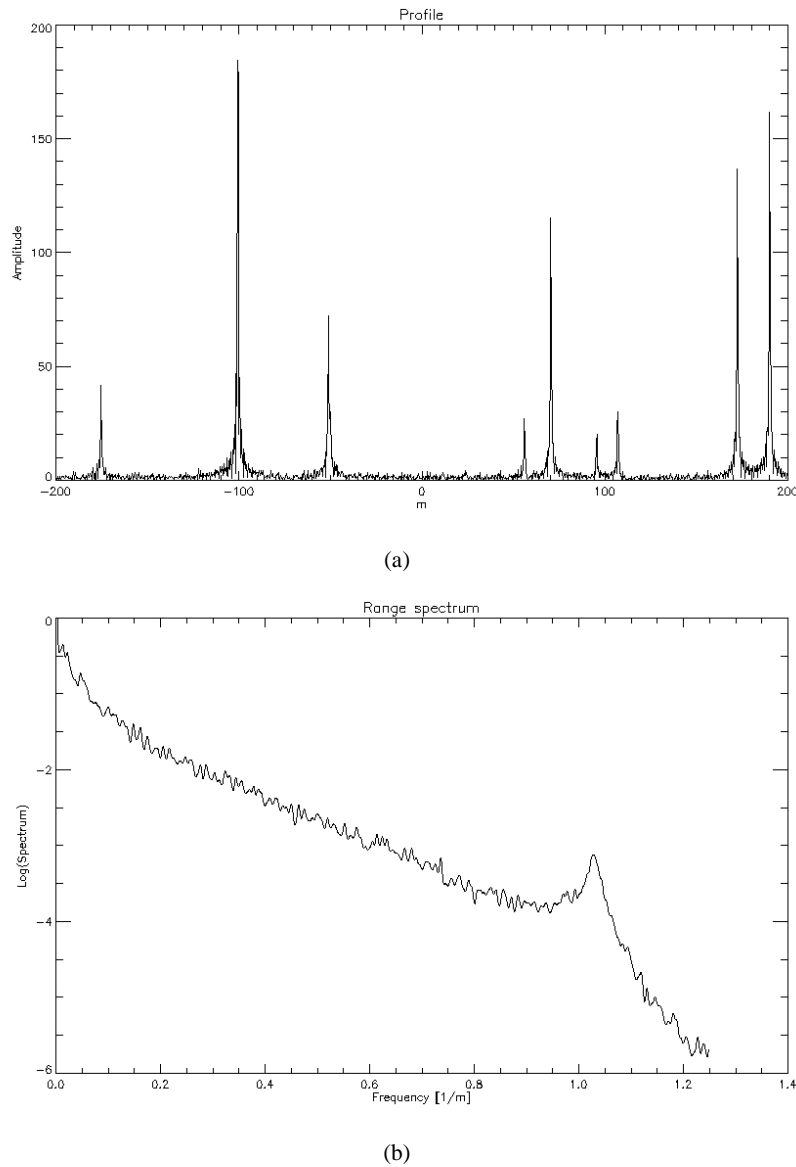


Fig. 2: Simulated amplitude profile for pointlike scatterers (a) and logarithmic plot of corresponding PSD (b).

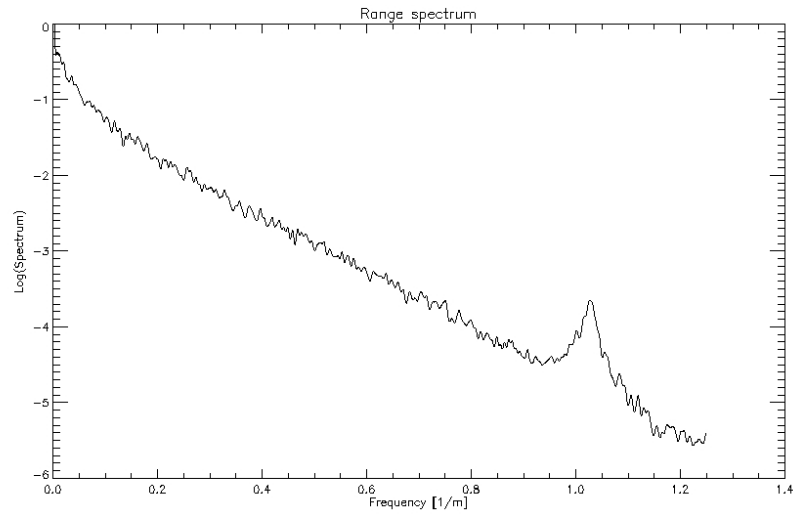


Fig. 3: Logarithmic plot of the PSD of simulated amplitude profiles for two-point scatterers.



Fig. 4: Subset of the COSMO/SkyMed enhanced spotlight 44° image containing the three considered study areas, the Forcella subset marked in green, the business district subset in blue, and the courthouse building layover in red. Near range is on the left.

In Fig. 5 we report the nine obtained plots of the PSDs organized in a sort of matrix: on the rows they are relevant to the same geographic area, while on the columns they are obtained from the same input image. The plots in Fig. 5 (a)-(c) are relevant to the area of Forcella, which consists essentially of historical buildings presenting a small number of floors; in the main, these buildings are not oriented along the sensor line of flight. This implies the presence on the scene of a limited number of pulses. In this case the obtained results are quite similar to the Fourier transform of the absolute value of the sinc and to the plot reported in Fig. 2 (b), apart from very high frequencies. In particular, the values of resolution and pixel spacing of the image acquired with a look angle of 44° are the same used in the previous simulation examples. Note that the slope of the graphs increases with the increase of the sensor look angle: this is due to the varying resolution, ranging from 0.375 m for the 22° image to 0.679 m for the 44° image, which implies the presence of pulses with increasingly larger widths.

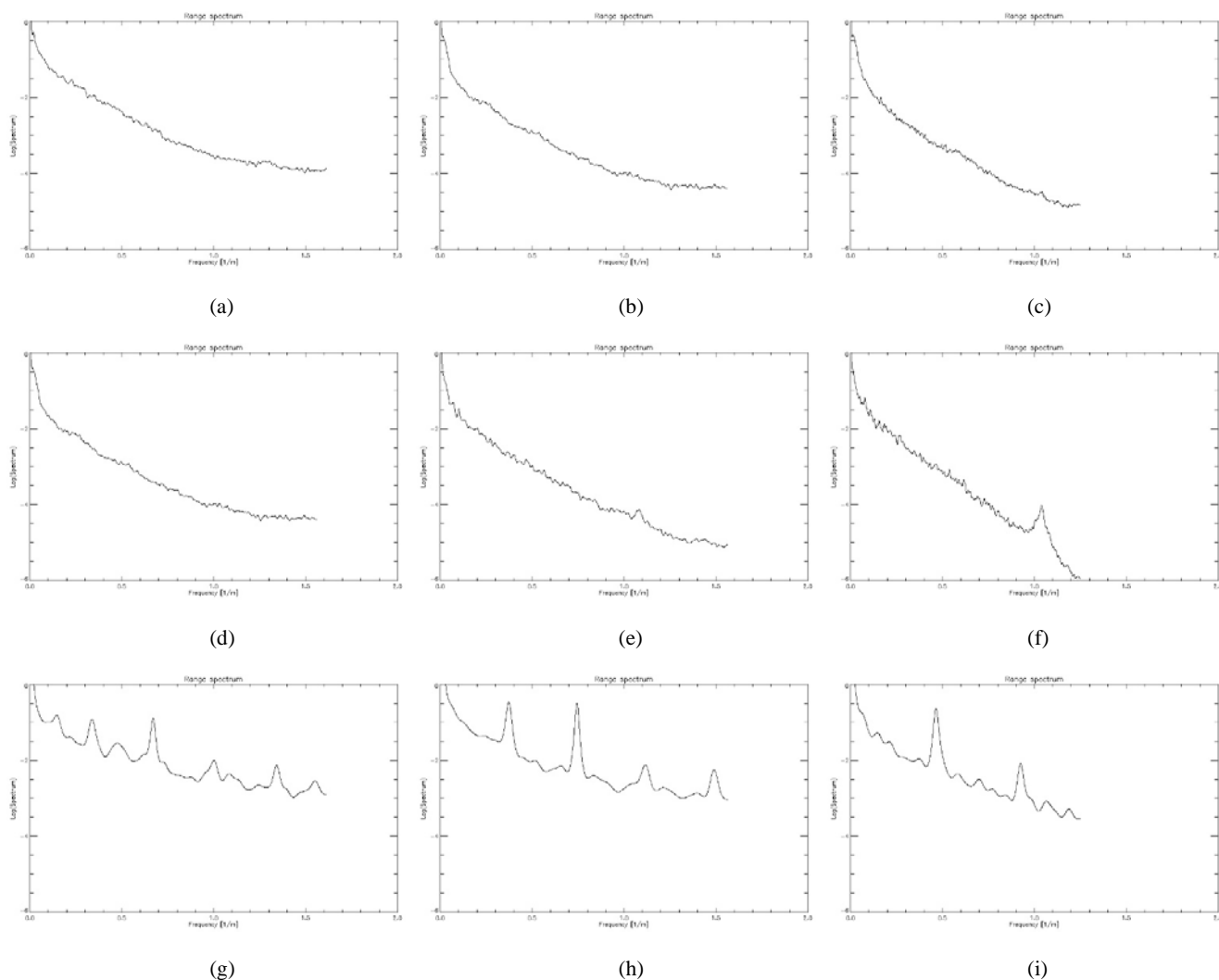


Fig. 5 Logarithmic plots of the range PSD of the three selected subsets: Forcella 22° (a), 31° (b), and 44° (c); business district 22° (d), 31° (e), and 44° (f); courthouse 22° (g), 31° (h), and 44° (i).

The plots in Fig. 5 (d)-(f) are relevant to the business district area. In this case the tall modern buildings present on the scene are mainly oriented along the sensor line of flight and are responsible for the presence of a large number of bright points and lines on the image (and hence high pulses in the profiles). The graphs are better approximated by a straight line and this is particularly evident in the case of Fig. 5 (f), i.e. for the 44° image, which resembles Fig. 3. Once again, for this image the width of the pulses is greater than for the other two. Note that, as expected (see Appendix), in Fig. 5 (e) and especially in Fig. 5 (f) a peak due to aliasing is present at frequency 1.12 m^{-1} and 1.03 m^{-1} , respectively; a peak would be expected also in Fig. 5 (d) at frequency 0.55 m^{-1} , however at this lower frequency the peak is hardly visible, because it is masked by the high value of the baseband spectrum.

The PSD relevant to the case of the courthouse is reported in Fig. 5 (g)-(i). The presence of spectral peaks is evident in this case. These peaks are mainly due to the presence of the periodic structure related to the building floors, as we will better highlight in the next section. We here just underline the similarity of Fig. 5 (i) and Fig. 1 (b).

Finally, some remarks on the spectra of the azimuth cuts of the images are in order. As an example, in Fig. 6 the logarithmic plots of the PSDs relevant to azimuth cuts of the three subsets of the 22° image are presented. The behavior is basically the same observed for the range cuts, except for a couple of meaningful differences. First, being the azimuth resolution practically the same for the three considered images, no significant variation in the PSDs is observed on images acquired with different look angles: for this reason, in Fig. 6 we report the results relevant to only one look angle. Moreover, as already noted (see Section II) the presence of periodic patterns related to the buildings is less frequent on azimuth cuts: in fact, in Fig. 6 (c) the azimuth PSD relevant to the case of the courthouse is reported, and no spectral peak is present, unlike in Fig. 5 (g)-(i), where the strong periodic signal components can be easily appreciated.

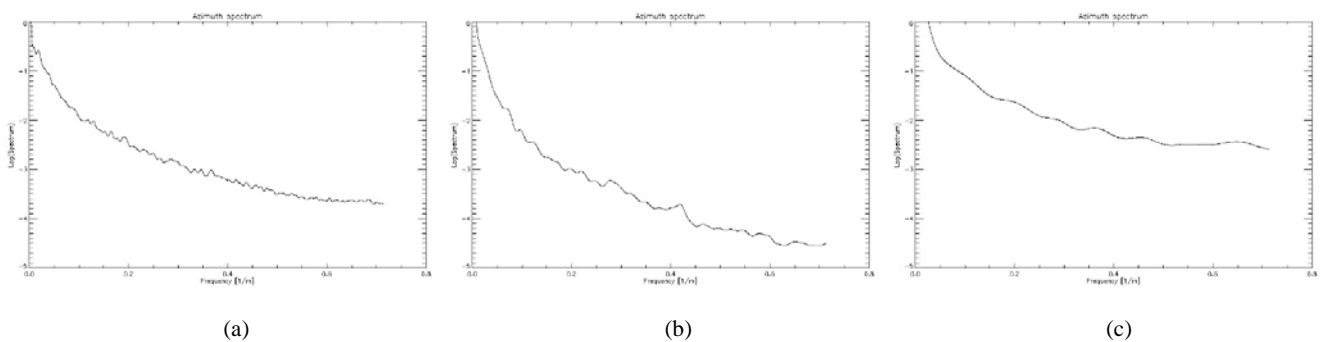


Fig. 6 Logarithmic plots of the azimuth PSD of the three selected subsets for the 22° image: Forcella (a); business district (b); courthouse (c).

IV. PARAMETER RETRIEVAL

The theoretical analysis of Section II and the experimental results of Section III suggest that some features of image spectra can be used to retrieve some parameters describing the imaged objects.

First of all, if we consider a portion of an image containing a building façade, then the positions of peaks in the range profile PSD can be used to retrieve the floor height, if we assume that the corresponding periodic pattern of bright lines or points is due to balconies and/or windows. In fact, (9) shows that the slant-range period d of the pattern can be obtained as

$$d = \frac{2\pi}{\eta_1} . \quad (12)$$

This slant-range period can be converted in a vertical period, i.e., a floor height h_{floor} , by dividing it by $\cos(\mathcal{G})$, where \mathcal{G} is the incidence angle (which must be known, as it is usually the case):

$$h_{floor} = \frac{d}{\cos \mathcal{G}} = \frac{2\pi}{\eta_1 \cos \mathcal{G}} . \quad (13)$$

Note that, while the direct evaluation of the floor height in the space domain is limited by the sensor geometric resolution, this frequency-domain estimate is only limited by the spectral estimator frequency resolution σ_η . The latter is of the order of $2\pi/L$, where L is the slant range length of the considered profile. Accordingly, the floor height precision $\sigma_{h_{floor}}$ is of the order of

$$\sigma_{h_{floor}} = \left| \frac{\partial}{\partial \eta} \left(\frac{2\pi}{\eta \cos \mathcal{G}} \right) \right| \sigma_\eta = \frac{2\pi}{\eta^2 \cos \mathcal{G}} \sigma_\eta \approx \frac{h_{floor}^2 \cos \mathcal{G}}{L} , \quad (14)$$

so that the relative height precision is of the order of the ratio of floor height and profile length, and the absolute height precision can be smaller or even much smaller than geometric resolution. Of course, many peaks may appear on the PSD, but one can select only those belonging to a spatial frequency range that corresponds to realistic floor heights (usually, 2 to 5 meters).

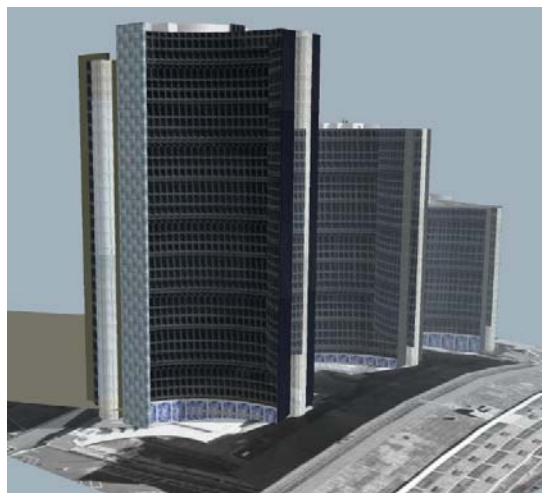
For instance, we can consider the images of the building layover of Fig. 4, whose estimated PSDs are reported in Fig. 5 (g)-(i) for different incidence angles. A Google SketchUp 3D model is available for this building and is reported in Fig. 7 (a), while in Fig. 7 (b) the layover extracted from the 44° image is shown. Periodic features related to the presence of the floor pattern are clearly visible on the image. From the estimated PSDs we evaluate the frequency location of the peaks present in the appropriate

TABLE I
ESTIMATED FLOOR HEIGHTS

	22°	31°	44°
f_i [m ⁻¹]	0.338	0.373	0.465
d [m]	2.96	2.68	2.15
h_{floor} [m]	3.25	3.24	3.31

range of frequencies typical of realistic floor heights. Note that we here use the spatial frequency f , which is related to the wavenumber through the expression $f = \eta / 2\pi$. Therefore, through (13) we can get an estimate of the floor height, using the appropriate values of the incidence angles (24.4°, 34.3°, and 49.5°). The obtained results are reported in Table I. The values obtained for h_{floor} in the three cases are very similar, with differences of the order of the electromagnetic wavelength. Moreover, the estimated values are very close to the one estimated from the available 3D model, i.e. 3.3 m.

Furthermore, it can be noted that some peaks may appear in the PSD, that are not related to true periodic patterns on the image, but are due to aliasing, see Appendix. However, positions of these peaks can be foreseen from knowledge of range resolution and pixel spacing (or, equivalently, chirp bandwidth and sampling frequency). In addition, this problem can be avoided by using intensity, rather than amplitude, images.



(a)



(b)

Fig. 7 Google SketchUp 3D model of the courthouse (a) and its layover extracted from the 44° amplitude SAR image (b).

Let us now move to other scene parameters. In principle the number M of floors of the building can be obtained as the ratio of peak position and width: in fact,

$$\frac{\eta_1}{\Delta\eta} = \frac{2\pi}{d} \cdot \frac{dM}{2\pi} = M \quad . \quad (15)$$

However, since the measured PSD peak shape may also depend on the employed spectral estimator, in this case it is more practical, and accurate, to directly retrieve the number of floors from the space-domain image.

Finally, let us consider cases in which the bright spots in the image are due to distributed targets or groups of very close pointlike scatterers. In this case, as verified in previous sections, the amplitude image PSD tends to be well approximated by an exponential function, and its logarithmic plot is approximated by a straight line. From (4) and (11) it is clear that the exponent of the PSD, and hence the slope of its logarithmic plot, is related to the size of the area covered by the group of scatterers. Accordingly, the latter can be retrieved by performing a linear regression of the PSD in a linear-log plane. Of course, if different groups of scatterers have different sizes, the obtained estimate must be considered as an averaged value of this size. For instance, for the 44° image the value of the exponent obtained through linear regression on the logarithmic plot of the PSD of the subset relevant to the business district is -3.59 , i.e. the width covered by the group of pulses is equal to about 1.8 m in slant range. Subtracting the slant range resolution $a=0.679$ m, we obtain that the size of the area covered by the group of scatterers is equal to about 1.1 m. This value is lower for the case of the Forcella subset, where the PSD exponent is equal to -2.96 , implying a width occupied by the group of pulses of 1.48 m in slant range, and a size of the area covered by the group of scatterers of about 0.8 m. Therefore, this parameter can be potentially used to characterize urban areas presenting different geometric (e.g. orientation with respect to the line of flight, wall depth) and electromagnetic features (e.g. complex dielectric constant).

V. CONCLUSIONS

In this paper, for the first time, a model of the PSD of amplitude (or intensity) VHR SAR images of urban areas has been presented. The model has been obtained by schematizing a VHR SAR amplitude image as a collection of spatially randomly distributed, sparse brilliant points, or lines, over a dark background, and possibly (if building façades are present and dominant) of bright features forming periodic spatial patterns. Obtained PSD expressions have been compared to measured PSDs of simulated and real range and azimuth profiles of VHR SAR amplitude images, and this comparison shows that measured PSDs are in reasonable agreement with theoretical model predictions. The presented model may be of interest *per se*; however, it also allows devising methods to extract some relevant scene parameters from measured PSD. As first examples, we have considered

the retrieval of building floor heights and of the average range size of small distributed targets. Of course, these spectral-domain methods can be used in conjunction with space-domain ones. Joint use of space- and spectral-domain retrieval schemes is matter of future work, as well as the automation of suggested retrieval algorithms, which at the moment still require the manual selection of the area of interest from the considered SAR image.

APPENDIX

In this Appendix we discuss the Fourier Transform of the absolute value of the sinc function,

$$p(r) = \left| \frac{\sin\left(\pi \frac{r}{a}\right)}{\pi \frac{r}{a}} \right|. \quad (16)$$

Since this function is real and even, also its Fourier Transform $P(\eta)$ is real and even. Unfortunately, it cannot be evaluated in closed form; however it can be shown that, due to the discontinuities of the derivative of $p(r)$ in $r_n = n a$, with n non-null integer, $P(\eta)$ is singular in $\eta_m = 2m\pi/a$, with m integer. In particular, $P(\eta)$ tends to $+\infty$ for $\eta \rightarrow 0$, and to $-\infty$ in all other singular points. A numerical evaluation of $P(\eta)$ is plotted in Fig. 8. This graph shows that, for $|\eta| > 2\pi/a$, $P(\eta)$ is negligible, except that in the vicinity of singular points, where it abruptly falls to $-\infty$. The presence of these sharp peaks at high frequencies may cause serious aliasing problems when $p(r)$ is sampled. In particular, given a sampling rate $\eta_s/(2\pi)$ included in the range from $1/2a$ to $1/a$, as it is usually the case, we have to expect an aliased peak at frequency $\eta_s/(2\pi) - 1/a$. For instance, if $a=0.679$ m and $\eta_s/(2\pi) = 1/0.4$ m⁻¹, as in the example of Section III, Figs. 2-3, then we have to expect an aliased peak at frequency $\eta_s/(2\pi) - 1/a \cong 1.03$ m⁻¹, which, in fact, is present in Figs. 2 (b) and 3.

Finally, in Fig. 9 we show the plot of $\log(|P(\eta)|^2)$ for $a = 0.679$ m to verify that, as foreseen by our theoretical model of Section II, the measured PSD of Fig. 2 (b), corresponding to a profile that is the collection of pointlike scatterers, is in very good agreement with the square modulus of the Fourier transform of a single pulse, except for the aliasing effect due to sampling.

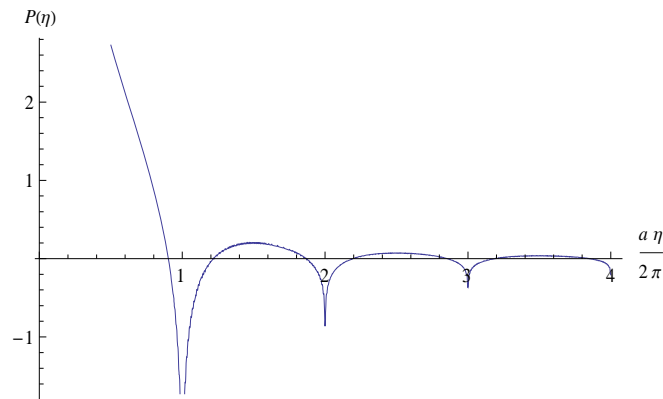


Fig. 8: Numerically evaluated Fourier Transform $P(\eta)$ of the absolute value of the sinc function of (16).

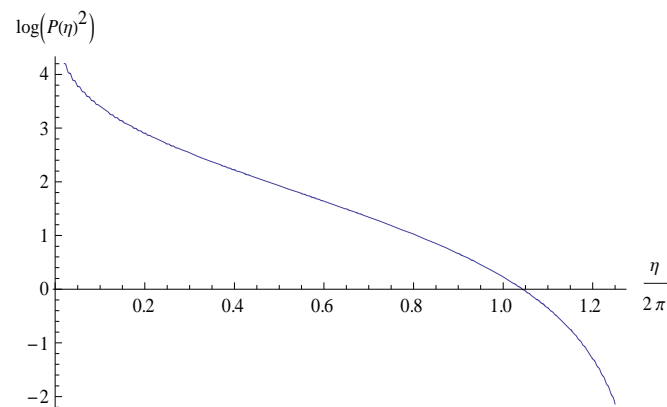


Fig. 9: Plot of $\log(|P(\eta)|^2)$ for $a = 0.679$ m.

REFERENCES

- [1] G. Franceschetti, A. Iodice, and D. Riccio, "A canonical problem in electromagnetic backscattering from buildings", *IEEE Trans. Geosc. Remote Sens.*, vol. 40, no. 8, pp. 1787-1801, Aug. 2002.
- [2] G. Franceschetti, A. Iodice, D. Riccio, and G. Ruello "SAR raw signal simulation for urban structures", *IEEE Trans. Geosc. Remote Sens.*, vol. 41, no. 9, pp. 1986-1995, Sept. 2003.
- [3] R. Guida, A. Iodice, D. Riccio, and U. Stilla, "Model-Based Interpretation of High-Resolution SAR Images of Buildings", *IEEE J. Sel. Topics Appl. Earth Obs. Remote Sens.*, vol. 1, no. 2, pp. 107-119, June 2008.
- [4] R. Guida, G. Franceschetti, A. Iodice, D. Riccio, G. Ruello, and U. Stilla, "Building feature extraction via a deterministic approach: Application to real high resolution SAR images" *Proc. Int. Geosci. Remote Sens. Symp.*, pp. 2681-2684, Barcelona, Spain, 2007.
- [5] R. Guida, A. Iodice, and D. Riccio, "Height Retrieval of Isolated Buildings from Single High Resolution SAR Images", *IEEE Trans. Geosc. Remote Sens.*, vol. 48, no. 7, pp. 2967-2979, July 2010.
- [6] S. Auer, S. Hinz, and R. Bamler, "Ray-Tracing Simulation Techniques for Understanding High-Resolution SAR Images," *IEEE Trans. Geosc. Remote Sens.*, vol. 48, no. 3, pp. 1445-1456, March 2010.

- [7] J. A. Benediktsson, M. Pesaresi, and K. Arnason, "Classification and Feature Extraction for Remote Sensing Images From Urban Areas Based on Morphological Transformations", *IEEE Trans. Geosc. Remote Sens.*, vol. 41, no. 9, pp. 1940-1949, Sept. 2003.
- [8] F. Dell'Acqua and P. Gamba, "Detection of urban structures in SAR images by robust fuzzy clustering algorithms: the examples of street tracking", *IEEE Trans. Geosc. Remote Sens.*, vol. 39, no. 10, pp. 2287-2297, Oct. 2001.
- [9] A. J. Bennett and D. Blacknell, "The Extraction of Building Dimensions from High Resolution SAR Imagery", *Proc. Int. Radar Conf.*, pp. 182-187, 2003.
- [10] R. Bolter, "Reconstruction of Man-Made Objects from High Resolution SAR Images", *IEEE Aerospace Conference Proceedings*, vol. 3, pp. 287-292, 2000.
- [11] F. Tupin, "Extraction of 3D information using overlay detection on SAR images", *Proceedings of the 2nd GRSS/ISPRS Joint Workshop on Remote Sensing and Data Fusion over Urban Areas*, pp. 72-76, Berlin (Germany), 2003.
- [12] V. Amberg, M. Coulon, P. Marthon, and M. Spigai, "Structure extraction from high resolution SAR data on urban areas", *Proc. Int. Geosci. Remote Sens. Symp.*, pp. 1784-1787, Toulouse (France), 2004.
- [13] P. Gamba, B. Houshmand, and M. Sacconi, "Detection and Extraction of Buildings from Interferometric SAR Data", *IEEE Trans. Geosc. Remote Sens.*, vol. 38, no. 1, pp. 611-618, Jan. 2000.
- [14] M. Quartulli and M. Datcu, "Information Fusion for Scene Understanding From Interferometric SAR Data in Urban Environments", *IEEE Trans. Geosc. Remote Sens.*, vol. 41, no. 9, pp. 1976-1985, Sept. 2003.
- [15] C. Tison, F. Tupin, and H. Maitre, "A fusion scheme for joint retrieval of urban height map and classification from high resolution interferometric SAR images," *IEEE Trans. Geosci. Remote Sens.*, vol. 45, no. 2, pp. 496-505, Feb. 2007.
- [16] A. Thiele, E. Cadario, K. Schulz, U. Thoennessen, and U. Soergel, "Building recognition from multi-aspect high-resolution InSAR data in urban areas," *IEEE Trans. Geosci. Remote Sens.*, vol. 45, no. 11, pp. 3583-3593, Nov. 2007.
- [17] C. Tison, F. Tupin, and H. Maitre, "Retrieval of building shapes from shadows in high resolution SAR interferometric images", *Proc. Int. Geosci. Remote Sens. Symp.*, pp. 1788-1791, Toulouse (France), 2004.
- [18] E. Simonetto, H. Oriot, and R. Garello, "Rectangular building extraction from stereoscopic airborne radar images", *IEEE Trans. Geosci. Remote Sens.*, vol. 43, n. 10, pp. 2386-2395, Oct. 2005.
- [19] F. Xu and Y.-Q. Jin, "Automatic reconstruction of building objects from multi-aspect metric-resolution SAR images," *IEEE Trans. Geosci. Remote Sens.*, vol. 45, no. 7 pp. 2336-2353, Jul. 2007.
- [20] F. Dell'Acqua, P. Gamba, and G. Lisini, "Improvements to Urban Area Characterization Using Multitemporal and Multiangle SAR Images", *IEEE Trans. Geosc. Remote Sens.*, vol. 41, no. 9, pp. 1996-2004, Sept. 2003.
- [21] M. Quartulli and M. Datcu, "Stochastic Geometrical Modeling for Built-Up Area Understanding from a Single SAR Intensity Image with Meter Resolution", *IEEE Trans. Geosc. Remote Sensing*, vol. 42, no. 9, pp. 1996-2003, Sept. 2004.
- [22] S. Auer, C. Gisinger, and R. Bamler, "Characterisation of SAR Image Patterns Pertinent to Individual Façades", *Proc. Int. Geosci. Remote Sens. Symp.*, pp. 3611-3614, Munich (Germany), 2012.
- [23] G. Di Martino, A. Iodice, D. Riccio, and G. Ruello, "Imaging of Fractal Profiles", *IEEE Trans. Geosci. Remote Sens.*, vol. 48, no. 8, pp. 3280-3289, Aug. 2010.
- [24] G. Di Martino, D. Riccio, and I. Zinno, "SAR Imaging of Fractal Surfaces", *IEEE Trans. Geosci. Remote Sens.*, vol. 50, no. 2, pp. 630-644, Feb. 2012.
- [25] S. M. Kay, *Modern Spectral Analysis*. Englewood Cliffs, NJ: Patience Hall, 1999.
- [26] J. Capon, "High-Resolution Frequency-Wavenumber Spectrum Analysis," *Proceedings of the IEEE*, vol. 57, no. 8, pp. 1408-1418, Aug. 1969.